ACS APPLIED MATERIALS & INTERFACES

Research Article

www.acsami.org

Enhanced Ethanol Sensing Characteristics of In_2O_3-Decorated NiO Hollow Nanostructures via Modulation of Hole Accumulation Layers

Hyo-Joong Kim,[†] Hyun-Mook Jeong,[†] Tae-Hyung Kim,[†] Jae-Ho Chung,[‡] Yun Chan Kang,[†] and Jong-Heun Lee*[,†]

[†]Department of Materials Science and Engineering, Korea University, Seoul 136-713, Republic of Korea

[‡]Department of Physics, Korea University, Seoul 136-713, Republic of Korea

Supporting Information

ABSTRACT: In this work, we report a dramatic enhancement in ethanol sensing characteristics of NiO hollow nanostructures via decoration with In_2O_3 nanoclusters. The pure NiO and 1.64−4.41 atom % In-doped NiO and In_2O_3-decorated NiO hollow spheres were prepared by ultrasonic spray pyrolysis, and their gas sensing characteristics were investigated. The response (the ratio between the resistance in gas and air) of the In_2O_3-decorated NiO hollow spheres to 5 ppm ethanol (C_2H_5OH) was 9.76 at 350 °C, which represents a significant improvement over the In-doped NiO and pure NiO hollow spheres (3.37 and 2.18, respectively). Furthermore, the 90% recovery time was drastically reduced from 1880 to 23 s, and a selective detection of ethanol with negligible cross-response to other gases was achieved. The enhanced gas response and fast recovery kinetics were explained in relation to the thinning of the near-surface hole accumulation layer of p-type NiO underneath n-type In_2O_3, the change of charge carrier concentration, and the variation of oxygen adsorption.

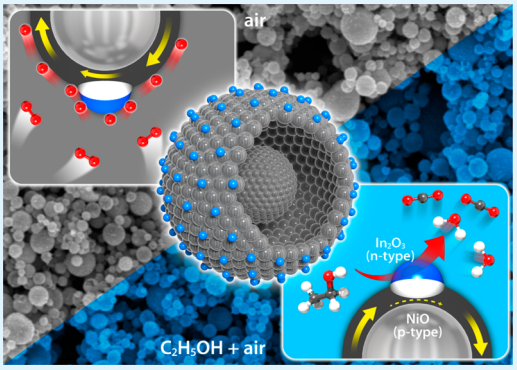

KEYWORDS: *gas sensor, hetero p−n junction, In_2O_3, sensitivity, recovery*

1. INTRODUCTION

Oxide semiconductor nanostructures have been widely used to detect harmful, toxic, and explosive gases[1−5] and can be broadly divided into two categories on the basis of their majority charge carrier. In n-type oxide semiconductors, the adsorption of negatively charged oxygen creates an electron depletion layer (EDL) near the surface;[1−4] thus, sensor resistance is determined by the serial connection between semiconducting cores and the resistive EDL. In p-type oxide semiconductors, on the other hand, the ionized adsorption of oxygen forms a hole accumulation layer (HAL) through electrostatic interaction between oppositely charged species (negatively charged oxygen and positively charged holes).[6−8] In this configuration, the sensor resistance is determined by parallel competition between conduction along the narrow cross-sectional area of the near-surface HAL and that across resistive cores with a relatively wide cross-sectional area.[6−8]

Generally speaking, the gas response of p-type oxide semiconductors is comparatively lower than that of n-type oxide semiconductors due to differences in their gas sensing mechanisms. This is supported by the calculation of Hübner et al., which demonstrates that the gas response of p-type oxide semiconductors is the square root of that of n-type oxide semiconductors with the same morphological configuration.[9] Nevertheless, p-type oxide semiconductors have a distinctive catalytic activity with various volatile organic compounds,[10−13] making them ideally suited to the design of new functionality in high-performance gas sensors. To achieve this, however, it is essential to first enhance the gas response of p-type oxide semiconductors.

Past approaches to enhancing the response and selectivity of n-type oxide semiconductor gas sensors have included the loading of noble metal catalysts (Pt, Pd, Rh, and Au),[14−17] controlling the charge carrier concentration,[18] and the formation of heterostructures.[19−21] The loading of noble metal catalysts[22−24] was also effective to improve or tune the gas sensing characteristics of p-type oxide semiconductors. Furthermore, it has been previously reported that the gas response of p-type NiO hollow spheres and nanofibers is significantly enhanced by doping with Fe^{3+},[25,26] as this reduces the hole concentration in the NiO sensor. However, the design of high-performance p-type oxide semiconductor gas sensors based on heteronanostructures is still very much in the early stages of investigation.

The present study evaluates the possibility of producing highly sensitive, selective, and rapidly recovering ethanol sensors through the decoration of p-type NiO hollow spheres with n-type In_2O_3 nanoclusters. The main focus of the study is

Received: August 4, 2014
Accepted: September 22, 2014
Published: September 22, 2014

directed toward understanding the gas sensing mechanism of these In_2O_3-decorated NiO hollow structures in relation to variations in the conduction path, oxygen adsorption, and space charge layer due to the establishment of a nanoscale p−n junction between NiO and In_2O_3.

2. EXPERIMENTAL SECTION

Preparation of NiO, In_2O_3-Decorated NiO, and In-Doped NiO Hollow Spheres. Nickel(II) nitrate hexahydrate ($Ni(NO_3)_2{\cdot}6H_2O$, 99.999% trace metals basis, Sigma-Aldrich) (1.452 g) and citric acid monohydrate ($C_6H_8O_7{\cdot}H_2O$, Sigma-Aldrich, 99%) (1.048 g) were dissolved in 500 mL of distilled water and stirred for 1 h. The solution was used to obtain particles via spray pyrolysis. Citric acid was added to induce the hollow morphology of spheres during spray pyrolysis.[27] The spray pyrolysis system used consisted of a droplet generator, quartz-tube reactor, and particle-collecting chamber. Six ultrasonic generators (resonant frequency: 1.7 MHz) were used to generate a plethora of droplets, which were subsequently carried into the high-temperature quartz-tube reactor (inner diameter: 55 mm) by a carrier gas (air, 40 L/min). The Ni-containing precursor spheres produced by pyrolysis were collected using a Teflon bag filter located in the particle-collecting chamber, which was held at a temperature of 250 °C to prevent the condensation of water. The reactor temperature was maintained at 700 °C, and the as-prepared precursor particles were heated at 600 °C for 2 h. For the sake of simplicity, the specimen prepared by spray pyrolysis and subsequent heat treatment is hereafter referred to as "NiO".

The NiO hollow spheres were drop-coated onto a silicon wafer that had been dried at 70 °C for 24 h. An alumina boat containing indium(II) chloride ($InCl_2$, 99.9%, Sigma-Aldrich) powder was then placed in the middle of the quartz tube of a horizontal tube furnace, and the silicon wafer coated in NiO hollow spheres was placed 5 cm downstream of this source material. After evacuating the quartz tube to $\sim 9 \times 10^{-2}$ Torr using a rotary pump, the furnace temperature was increased to 350 °C and held for 20 min to produce indium-decorated NiO hollow spheres through a reaction between the source and an Ar−O_2 gas mixture gas (Ar, 100 sccm; O_2, 1 sccm). Owing to the fact that the reaction temperature was higher than the melting temperature of the $InCl_3$ source, indium-containing nanoparticles were grown on the NiO hollow spheres by means of a vapor−liquid−solid mechanism. After heat treatment at 600 °C for 2 h, In_2O_3-decorated NiO hollow spheres were produced that shall be referred to as "In_2O_3-NiO".

In order to investigate the effect that the phase and configuration of the In component has on the gas sensing characteristics of the NiO hollow spheres, In-doped NiO hollow spheres were also prepared through spray pyrolysis of stock solutions (solvent: distilled water 500 mL) containing various amounts of indium(III) nitrate hydrate ($In(NO_3)_3{\cdot}xH_2O$, 99.9% metals basis, Sigma-Aldrich), nickel(II) nitrate hexahydrate, and citric acid monohydrate. The indium composition of the In-doped NiO hollow spheres prepared from the solutions with In/Ni ratios of 2 and 5 atom % were determined to be 1.64 and 4.41 atom %, respectively, by inductively coupled plasma mass spectroscopy. These specimens are referred to as "1.64In-NiO" and "4.41In-NiO".

Characterization. The phase and crystallinity of the powders were analyzed by X-ray diffractometry (XRD, D/MAX-2500 V/PC, Rigaku, Japan), while the morphologies of the precursors and hollow powders were investigated by field emission scanning electron microscopy (FESEM, S-4800, Hitachi Co. Ltd., Japan) and transmission electron microscopy (TEM, FEI TITAN 80-300TM, FEI Co., USA). The chemical state of each sample was examined by X-ray photoelectron spectroscopy (XPS, Multi Lab 2000, Thermo Scientific, USA). Inductively coupled plasma-atomic emission spectroscopy (ICP-AES, OPTIMA 4300 DV, PerkinElmer Instruments, USA) was used to determine the In-doping concentration in the NiO hierarchical nanostructures.

Gas Sensing Characteristics. Alumina substrates (area = 1.5 mm × 1.5 mm; thickness = 0.25 mm) with two Au electrodes on the upper surface (electrode widths = 1 mm; separation = 0.2 mm) and a micro heater on the lower surface were drop-coated with slurries of NiO, 1.64In-NiO, 4.41In-NiO, and In_2O_3-NiO hollow spheres dispersed in deionized water using a micropipette. The sensor temperatures were controlled using the micro heater and were measured using an IR temperature sensor (Metis MP25, Sensortherm GmBH, Germany). The substrate temperature was controlled between 325 and 475 °C by adjusting the heater powers in the range of 248−419 mW. The sensors were contained in a specially designed, low-volume (1.5 cm^3) quartz tube to minimize any delay in changing their surrounding atmosphere. Following the removal of residual solvent by heating the sensor at 500 °C for 24 h, the gas responses ($S = R_g/R_a$, R_g: resistance in gas, R_a: resistance in air) to 5 ppm benzene (C_6H_6), *o*-xylene (1,2-dimethylbenzene, $C_6H_4(CH_3)_2$), formaldehyde (HCHO), ethanol (C_2H_5OH), ammonia (NH_3), carbon monoxide (CO), and hydrogen (H_2) were measured at 325−475 °C. The gas concentrations were controlled by changing the mixing ratio of the parent gases and dry synthetic air. The DC two-probe resistances were measured using an electrometer interfaced with a computer.

3. RESULTS AND DISCUSSION

Phase, Composition, and Morphological Properties of NiO, In-NiO, and In_2O_3-NiO. The spherical morphology of the Ni-precursors prepared by ultrasonic spay pyrolysis was maintained after heat treatment at 600 °C for 2 h (Figure S1a, Supporting Information). Most of the NiO spheres consisted of a thin shell (diameter: 200−500 nm; thickness: 24.5 ± 4.2 nm) surrounding a yolk (diameter: 153.2 ± 48.2 nm), although some hollow spheres without a yolk were also observed. The 1.64In-NiO (Figure S1b, Supporting Information) and 4.41In-NiO (Figure S1c, Supporting Information) also formed as yolk−shell spheres with very similar shell thicknesses and yolk sizes. A uniform distribution of In was confirmed within both the 1.64In-NiO (Figure S2a, Supporting Information) and 4.41In-NiO (Figure S2b, Supporting Information) specimens by energy dispersive spectroscopy (EDS) elemental mapping.

The In_2O_3-NiO hollow spheres were prepared by coating In onto hollow NiO spheres by chemical vapor deposition (CVD), followed by heat treatment at 600 °C for 2 h (Figure 1a,b), which retained both the yolk−shell morphology and shell thickness (Figure 1c). The (222) lattice fringes of In_2O_3 (separated by 2.921 Å) and (101) lattice fringes of NiO (separated by 2.412 Å) were observed near the surface of the spheres (Figure 1d and Figure S3b, 3d, Supporting Information), indicating the presence of In_2O_3 nanoparticles in a discrete manner on NiO spheres. The EDS elemental mapping results in Figure 1e also clearly show that In is present over the entire NiO sphere surface. The average In concentration across 14 different points on the shell was found to be 3.33 ± 0.94 atom %, which is substantially higher than the values obtained from 7 different locations within the core (1.09 ± 0.57 atom %) (Figure S4, Supporting Information). This indicates that most of the In does not diffuse into the core yolk but rather remains as a coating on the NiO hollow sphere shell.

Following heat treatment at 600 °C for 2 h, the NiO, 1.64In-NiO, 4.41In-NiO, and In_2O_3-NiO hollow spheres all exhibited very similar XRD patterns for their respective NiO phase (JCPDS# 47-1049) (Figure 2). Moreover, there were no secondary phases evident in any of the 1.64In-NiO, 4.41In-NiO, and In_2O_3-NiO hollow spheres (Figure 2b−d), and this absence of In-related peaks can be attributed either to the incorporation of In into the NiO lattice or to the presence of a secondary phase that is simply below the detection limit of X-ray diffraction. The precise positions of the (101), (012), (110),

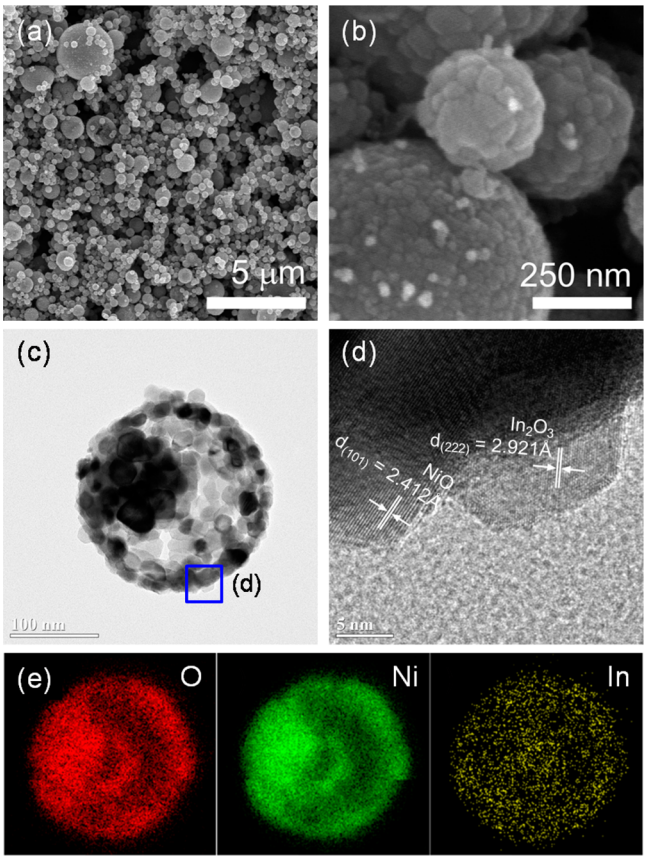

Figure 1. (a,b) SEM and (c,d) TEM images of In_2O_3-NiO hollow spheres after heat treatment at 600 °C for 2 h and (e) EDS elemental mapping images of O, Ni, and In components.

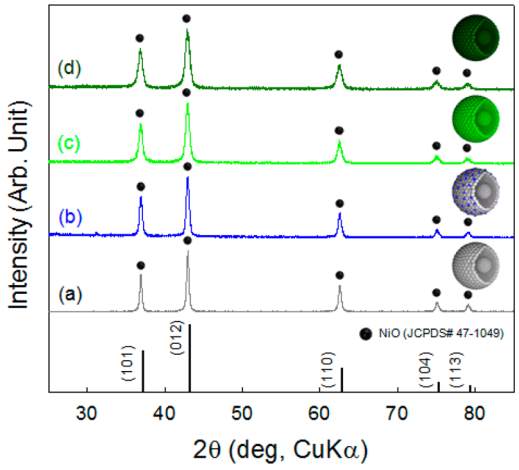

Figure 2. X-ray diffraction patterns of (a) NiO, (b) In_2O_3-NiO, (c) 1.64In-NiO, and (d) 4.41In-NiO hollow spheres after heat treatment at 600 °C for 2 h.

(104), and (113) peaks were obtained by performing a Rietveld refinement of the full profiles using the General Structure Analysis System (GSAS) program.[28] As a result of this, all peaks in the 1.64In-NiO and 4.41In-NiO hollow spheres shifted to lower angles (Figure S5, Supporting Information), and the lattice parameters were found to increase with In-doping (the lattice parameter of NiO = 4.17723 ± 0.00004 Å, 1.64In-NiO = 4.17840 ± 0.00031 Å, and 4.41In-NiO = 4.18018 ± 0.00010 Å). Given that the ionic radius of In^{3+} with a coordination number of 6 is 0.80 Å, while that of Ni^{2+} with a coordination number of 6 is 0.69 Å, this peak shift and increase in lattice parameter can be attributed to the substitution of In^{3+} at Ni^{2+} sites. In contrast, the peak positions and lattice parameters of the In_2O_3-NiO hollow spheres were similar to those of the NiO hollow spheres, indicating the formation of a nanocomposite between In_2O_3 and NiO.

The specimens were further analyzed using XPS to investigate the incorporation of In in NiO, the formation of an In_2O_3-NiO heterocomposite, and the physicochemical states of the samples. The fine-scan XPS spectra for Ni $2p_{3/2}$ are shown in Figure 3a–d, in which both Ni^{2+} and Ni^{3+} bonding structures can be clearly observed at 853.7 and 855.0 eV, respectively. From a fitting using the Voigt amp method, the Ni^{2+}/Ni^{3+} ratio of the NiO specimens was determined to be 1.45 (Figure 3a). This indicates that 59.2 atom % of the Ni forms an ionic bond with lattice oxygen (Ni–O) and a small amount of Ni (40.8 atom %) ions exists in an oxidized state near the surface (Ni_2O_3).[29] The substitution of In^{3+} at Ni^{2+} sites, and consequent charge compensation, can be described as follows:

$$In_2O_3 + 2h^{\bullet} \xrightarrow{2NiO} 2In_{Ni}^{\bullet} + 2O_O^{X} + \frac{1}{2}O_2(g) \quad (1)$$

This shows a decrease in the hole concentration of p-type NiO semiconductors as a result of In_2O_3 doping. It should be noted that the Ni^{2+}/Ni^{3+} ratio decreases to 0.43 when the In content is increased to 4.41 atom % (Figure 3c,d). The adsorption of negatively charged oxygen on the surface of NiO is known to occur through a change of Ni^{2+} into Ni^{3+},[30] but it has also been reported that Ni^{3+} can be formed from negatively charged interstitial oxygen (O_i'').[31] Accordingly, the decrease observed in the Ni^{2+}/Ni^{3+} ratio with In-doping can be explained by the conversion of oxygen molecules generated by the incorporation reaction in eq 1 into negatively charged interstitial (or surface) oxygen through the oxidation of Ni^{2+} into Ni^{3+}.

$$\frac{1}{2}O_2(g) + 2NiO \xrightarrow{2NiO} O_i'' + 2Ni_{Ni}^{\bullet} + 2O_O^{X} \quad (2)$$

It should be noted here that the Ni^{2+}/Ni^{3+} ratio (0.91) of the In_2O_3-NiO sample containing 3.88 atom % In was substantially higher than the 1.64In-NiO sample (Ni^{2+}/Ni^{3+} = 0.51) but lower than the NiO sample (Ni^{2+}/Ni^{3+} = 1.45) (Figure 3b). This indicates that at least some of the In was incorporated into the NiO lattice, but most of it was present as a secondary phase (In_2O_3).

The In $3d_{5/2}$ peaks of the In-doped NiO and In_2O_3-decorated NiO specimens were observed at 443.8–443.9 and 444.3 eV, respectively, (Figure 3f–h), with the low binding energy of the 1.64In-NiO and 4.41In-NiO specimens (Figure 3g,h) indicative of In having bonded with lattice oxygen. In contrast, the high binding energy (444.3 eV) of the In_2O_3-NiO specimen (Figure 3f) indicates bonding between In and either –OH or moisture in the air.[32,33] The O 1s peak of NiO at 529.3 eV was symmetric in shape (Figure 3i), whereas the equivalent peaks of 1.64In-NiO, 4.41In-NiO, and In_2O_3-NiO hollow spheres were asymmetric (Figure 3j–l). The O 1s peaks will be analyzed further in relation to the gas sensing mechanism in the later section.

Gas Sensing Characteristics. The dynamic sensing transients of sensors based on NiO, In-doped NiO, or In_2O_3-decorated NiO hollow spheres to 5 ppm ethanol were

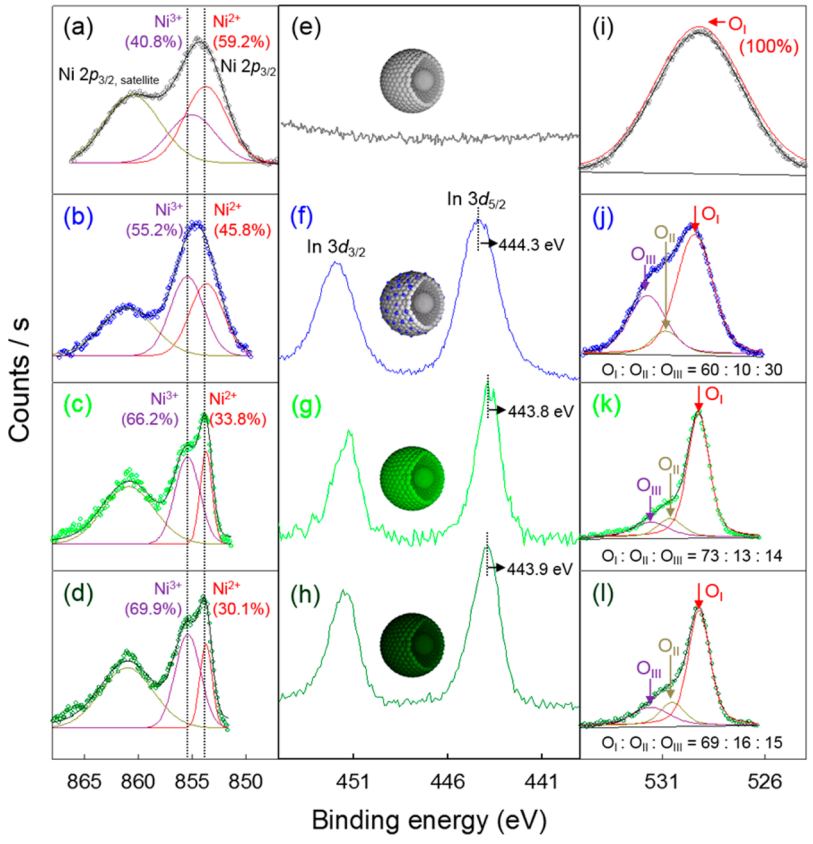

Figure 3. XPS spectra of (a,e,i) NiO, (b,f,j) In_2O_3-NiO, (c,g,k) 1.64In-NiO, and (d,h,l) 4.41In-NiO hollow spheres after heat treatment at 600 °C for 2 h. (a–d) Ni 2p, (e–h) In 3d, and (i–l) O 1s peaks and fitting analysis.

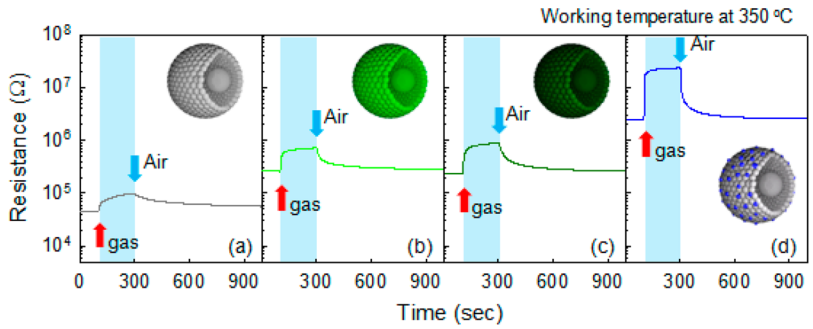

Figure 4. Dynamic sensing transient of (a) NiO, (b) 1.64In-NiO, (c) 4.41In-NiO, and (d) In_2O_3-NiO sensors to 5 ppm ethanol at 350 °C.

measured at 325–475 °C (Figure 4 and Figure S6, Supporting Information). All the sensors exhibit a chemiresistive variation that is typical of p-type oxide semiconductors: there is an increase and decrease in sensor resistance upon exposure to a reducing gas and air, respectively. This indicates that conduction in In_2O_3-decorated NiO spheres does not occur along the discrete configuration of n-type In_2O_3 nanoclusters but rather through the p-type NiO spheres and shows that In-doped NiO spheres are a p-type oxide semiconductor.

The responses of the various sensors to 5 ppm ethanol were measured at 325–475 °C, the results of which are summarized in Figure 5. From this, we see that a pure NiO sensor has the lowest response (Figure 5a1), and this can only be slightly increased by In-doping alone (Figure 5a2,a3). However, the gas response of the In_2O_3-NiO sensors is significantly higher than the other three sensors (Figure 5a4), indicating that the gas response of NiO sensors is highly dependent upon the configuration of the In component. The resistance in air (R_a) was also measured for each sensor (Figure 5b1–b4), revealing that the R_a values for 1.64In-NiO and 4.41In-NiO sensors are similar, but substantially higher, than that of a NiO sensor. This can be ascribed to the incorporation of In^{3+} into NiO and the subsequent decrease in hole concentration. The slight decrease in R_a that resulted from increasing the In-doping concentration from 1.64 to 4.41 atom % was attributed to the difference in the thickness of the sensing film. Interestingly, despite its low In concentration (3.88 atom %), the R_a value of the In_2O_3-NiO sensor is significantly higher than the 1.64In-NiO and 4.41In-NiO sensors. This strongly indicates that the In component has a different configuration or phase. Considering the results of TEM and XPS, it is considered to be a hetero p–n junction between In_2O_3 and NiO that increases the sensor resistance. However, even in the In_2O_3-NiO specimen, the small amount of In-doping of the NiO lattice needs to also be taken into

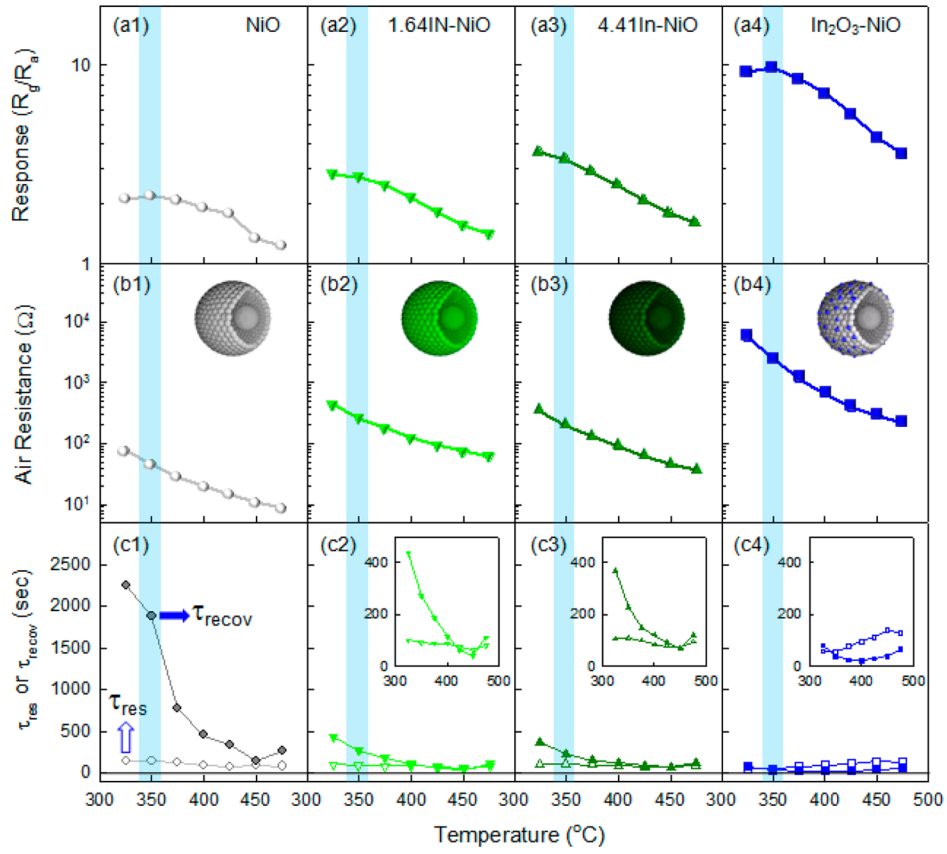

Figure 5. (a) Gas response to 5 ppm ethanol, (b) sensor resistance in air, and (c) 90% response and 90% recovery time (τ_{res} and τ_{recov}) of NiO, 1.64In-NiO, 4.41In-NiO, and In_2O_3-NiO sensors at 325−475 °C.

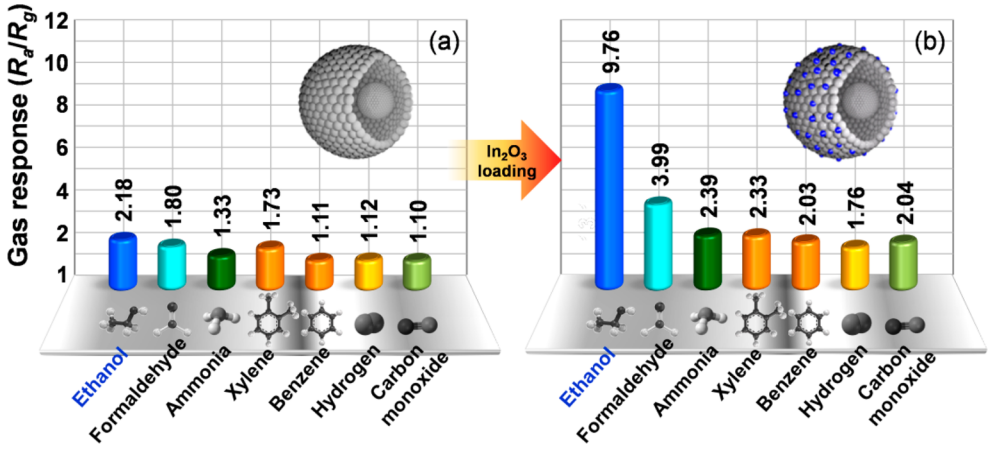

Figure 6. Gas response of (a) NiO and (b) In_2O_3-NiO sensors to 5 ppm ethanol, formaldehyde, ammonia, *o*-xylene, benzene, hydrogen, and carbon monoxide at 350 °C.

account as a possible reason for the increased sensor resistance due to the change that this induces in the Ni^{2+}/Ni^{3+} ratio.

The times to reach 90% variation in resistance upon exposure to ethanol and air were defined as the 90% response time (τ_{res}) and 90% recovery time (τ_{recov}), respectively. All sensors showed similar τ_{res} values (60−150 s) upon exposure to 5 ppm ethanol (Figure 5c1−c4), yet their τ_{recov} values were significantly different. Significantly, the pure NiO sensors showed a prolonged recovery time (e.g., τ_{recov} = 1880 s at 350 °C), whereas a greatly reduced τ_{recov} value was obtained with the 1.64In-NiO (272 s) and 4.41In-NiO sensors (228 s) that was even further reduced to just 23 s in In_2O_3-NiO sensors. These tendencies were maintained across all sensor temperatures tested, although the difference in τ_{recov} did become smaller at higher temperatures due to thermal promotion of the recovery reaction. This indicates that the recovery reaction involving the in-diffusion, adsorption, dissociation, and ionization of oxygen on the surface takes prolonged time in NiO sensors and is critically dependent on the configuration of the In component in In-doped or In_2O_3-decorated NiO sensors.

The dynamic sensing transient of the In_2O_3-NiO sensor to 2−100 ppm ethanol was measured at 350 °C (Figure S7, Supporting Information) and demonstrated stable sensing and recovery characteristics. The response to 2 ppm ethanol was

dx.doi.org/10.1021/am5051923 | ACS Appl. Mater. Interfaces 2014, 6, 18197−18204

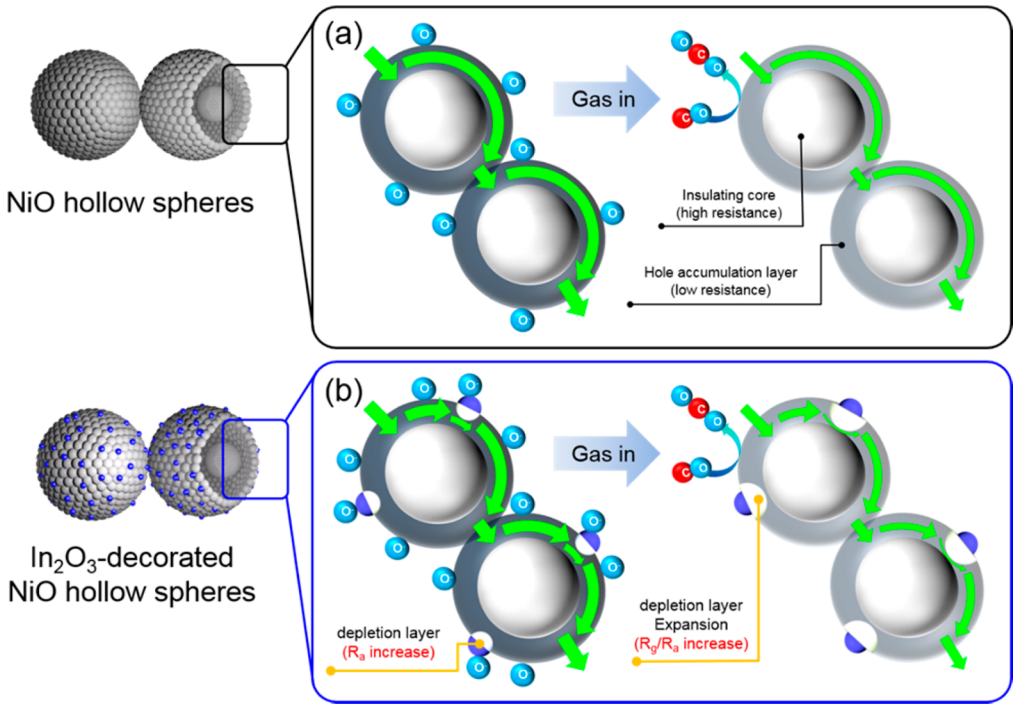

Figure 7. Gas sensing mechanisms of (a) NiO and (b) In_2O_3-NiO hollow spheres.

6.88 (inset of Figure S7, Supporting Information), indicating that the present sensor can detect subppm levels of ethanol. The selectivity against other interference gases was also checked by measuring the responses to 5 ppm ethanol, formaldehyde, ammonia, xylene, benzene, hydrogen, and carbon monoxide at 350 °C (Figure 6). The responses of the NiO sensor did not show any significant selectivity to a specific gas (Figure 6a), whereas the response of the In_2O_3-NiO sensor to 5 ppm ethanol (R_g/R_a = 9.76) was markedly higher than those to formaldehyde, ammonia, xylene, benzene, hydrogen, or carbon monoxide (R_g/R_a = 1.76−3.99) (Figure 6b). This demonstrates that ethanol can be selectively and sensitively detected using an In_2O_3-NiO sensor.

Gas sensing mechanisms of NiO and In_2O_3-NiO sensors are shown in Figure 7. The sensor resistance of p-type oxide semiconductors is increased upon exposure to a reducing gas, as the oxidation of this gas by negatively charged oxygen generates electrons that reduce the hole concentration in the shell layer through the electron−hole recombination (Figure 7a). In this study, the ethanol responses of 1.64In-NiO, 4.41In-NiO, and In_2O_3-NiO hollow spheres were found to be higher than those of pure NiO hollow spheres; however, it should be noted that the variation in hole concentration due to the gas sensing reaction will lead to a higher variation in sensor resistance when the background hole concentration is lower. Indeed, it has previously been confirmed that both the sensor resistance and gas response of NiO nanostructures is significantly enhanced by doping with Fe^{3+}.[25,26] Accordingly, in the case of In-doped NiO hollow spheres, the increase in gas response and sensor resistance can be explained by a reduced hole concentration in the sensing materials due to In^{3+} doping.

The significant enhancement in gas response achieved by decorating p-type NiO hollow spheres with n-type In_2O_3 can be attributed to the formation of nanoscale p−n junctions. The formation of the hole depletion layer underneath the n-type In_2O_3 nanoclusters will narrow the hole accumulation layer for conduction, which provides an explanation for the higher resistance of the In_2O_3-NiO sensor in Figure 5b (left diagram in Figure 7b). Moreover, considering the small amount of In-doping identified in the In_2O_3-NiO sensor by XPS analysis, one can expect a decrease in the hole concentration at the hole accumulation layer in In_2O_3-NiO hollow spheres. Note that the widths of the space charge layer in the n- and p-oxide semiconductor sides (w_N and w_P) are also dependent upon the relative ratio of the charge carrier concentration (N_D/N_A; N_D: donor density; N_A: acceptor density).

$$w_N N_D = w_P N_A \quad (3)$$

Given that the w_P value will increase as N_A decreases, In-doping not only reduces the hole concentration within the hole accumulation layer but also makes the hole depletion layer underneath the n-In_2O_3 nanoclusters thicker. This, in turn, causes the p-conducting channel under the hole depletion layer to narrow; thus, a small change in charge carrier concentration can lead to higher variation in sensor resistance (Figure 7b). The above gas sensing mechanism indicates that the optimum concentration of n-In_2O_3 nanoclusters for the maximum gas response of p-type oxide nanostructures is not fixed but depends on the thickness of p-type oxide nanostructures, the size/dispersion of n-In_2O_3 nanoclusters, and the contact configuration between n- and p-type oxide nanostructures. In the literature, n−n heteronanostructures using two oxide semiconductors with different band gaps, electron affinities, and work functions are also used to enhance the gas response by the modulation of energy band bending and built-in potential.[34,35] In this perspective, p−p heteronanostructures using two different oxides with different energy band structures can be also considered in the of design high performance gas sensors. That is, the gas response of p-type oxide semiconductor sensors can be effectively controlled or tuned by varying the decoration of n-type or different p-type oxide semiconductor nanoclusters.

It should be noted that the recovery time at <400 °C is significantly shortened by decorating NiO with In_2O_3 nanoclusters or doping it with In (Figure 5c4). The recovery reaction incorporates the in-diffusion, adsorption, dissociation, and ionization of oxygen; thus, the similarity in the τ_{res} value between the sensors in Figure 5c reflects the fact that the gas diffusion is not a critical parameter in determining the recovery rate. Instead, the recovery kinetics needs to be understood within the framework of oxygen adsorption and ionization. To this end, the O 1s peaks of the 1.64In-NiO, 4.41In-NiO, and In_2O_3-NiO specimens (Figure 3j–l) were deconvoluted into three different contributions:[36,37] lattice oxygen (O_I: 529.4 eV), terminal layer of oxygen (O_{II}: 530.8 eV), and chemisorbed oxygen and water related species (O_{III}: 531.7 eV). The chemisorbed oxygen species at high sensing temperature turn into −OH or water related species at room temperature for XPS analysis. Thus, the intensity of the O_{III} peak is closely related to the chemisorption of oxygen. Although only lattice oxygen (O_I) is observed in pure NiO (Figure 3i), substantial contributions of the terminal layer of oxygen (O_{II}) are evident in 1.64In-NiO, 4.41In-NiO, and In_2O_3-NiO sensors. Moreover, a large amount of O_{III} is observed in In_2O_3-NiO sensors. Golovanov et al.[37] reported that the coverage of surface bridging oxygen on the (400) surface of In_2O_3 is significantly higher when two different types of oxygen species coexist (e.g., O_I + O_{II}, O_I + O_{III}, and O_{II} + O_{III}), with the lowest surface energy obtained with the coexistence of O_{II} and O_{III}. Note that this abundance of oxygen species adsorbed on the surface of In_2O_3 can be transferred to the surface of NiO, thereby promoting the oxygen-adsorption-based recovery of the NiO surface. Indeed, the In_2O_3-NiO sensor with the largest amount of O_{II} + O_{III} showed the fastest recovery and is further supported by the faster recoveries of 1.64In-NiO and 4.41In-NiO sensors with substantial O_{II} and O_{III} than that of NiO sensors without O_{II} and O_{III}. Put simply, both the In-doping and In_2O_3 decoration are an effective approach to achieve fast recovering NiO-based sensors.

The responses of NiO hollow spheres decorated with In_2O_3 nanoclusters to 50−100 ppm C_2H_5OH (S = 21.9−25.1) are significantly higher than those (S = 1.8−5.5) of various morphology of NiO nanostructures in the literature.[24,25,38−45] In this perspective, the modulation of hole accumulation layer in NiO hollow spheres by the decoration of In_2O_3 nanoclusters provides a new and promising strategy to design high performance C_2H_5OH sensor with high response, superior selectivity, and fast response/recovery.

4. CONCLUSION

Highly sensitive, selective, and rapidly recovering ethanol sensors were designed by the modulation of hole accumulation layer in p-type NiO hollow spheres via coating the n-In_2O_3 nanoparticles. The gas sensing characteristics of In-doped and In_2O_3-decorated NiO hollow spheres were significantly different from those of pure NiO hollow spheres. The 1.64 and 4.41 atom % In-doping increases the sensor resistance and gas response due to a reduced hole concentration in NiO. The greatest enhancement in gas response to 5 ppm ethanol and sensor resistance in air was obtained by decorating NiO hollow spheres with In_2O_3 nanoclusters, an effect which was attributed to a thinning of the near-surface hole accumulation layer by the radial extension of the hole depletion layer underneath the n-type In_2O_3 nanoclusters. A high selectivity to ethanol was also obtained in this In_2O_3-decorated NiO sensor. Moreover, the recovery speed of the sensor was significantly enhanced by the decoration of In_2O_3 nanoclusters with abundant oxygen adsorption. This dual-role nature of In_2O_3 nanoclusters on NiO hollow spheres therefore provides a new and novel approach to designing highly sensitive, selective, and rapidly recovering gas sensors based on p-type oxide semiconductors.

■ ASSOCIATED CONTENT

Supporting Information

SEM and TEM images of NiO and In-doped NiO hollow spheres; TEM elemental mapping of In-doped NiO hollow spheres; TEM image of In_2O_3-decorated NiO hollow spheres; TEM EDS analysis of In_2O_3-NiO; peak shift in XRD analysis; gas sensing characteristics at 325−475 °C; dynamic sensing transient of In_2O_3-NiO hollow spheres to ethanol at 350 °C. This material is available free of charge via the Internet at http://pubs.acs.org.

■ AUTHOR INFORMATION

Corresponding Author

*E-mail: jongheun@korea.ac.kr. Fax: +82-2-928-3584. Tel: +82-2-3290-3282.

Notes

The authors declare no competing financial interest.

■ ACKNOWLEDGMENTS

This work was supported by a National Research Foundation of Korea (NRF) grant funded by the Korea government (MEST) (No. 2013R1A2A1A01006545).

■ REFERENCES

(1) Yamazoe, N. Toward Innovations of Gas Sensor Technology. *Sens. Actuators, B: Chem.* **2005**, *108*, 2−14.
(2) Shimizu, Y.; Egashira, M. Basic Aspects and Challenges of Semiconductor Gas Sensors. *MRS Bull.* **1999**, *24*, 18−24.
(3) Kolmakov, A.; Moskovits, M. Chemical Sensing and Catalyst by One-Dimensional Metal Oxide Nanostructures. *Annu. Rev. Mater. Res.* **2004**, *34*, 151−180.
(4) Barsan, N.; Weimer, U. Conduction Model of Metal Oxide Gas Sensors. *J. Electroceram.* **2001**, *7*, 143−167.
(5) Arafat, M. M.; Haseeb, A. S. M. A.; Akbar, S. A. A Selective Ultrahigh Responding High Temperature Ethanol Sensor Using TiO_2 Nanoparticles. *Sensors* **2014**, *14*, 13613−13627.
(6) Barsan, N.; Simion, C. E.; Heine, T.; Pokhel, S.; Weimar, U. Modeling of Sensing and Transduction for P-Type Semiconducting Metal Oxide Based Gas Sensors. *J. Electroceram.* **2010**, *25*, 11−19.
(7) Kim, H.-J.; Lee, J.-H. Highly Sensitive and Selective Gas Sensors Using P-Type Oxide Semiconductors: Overview. *Sens. Actuators, B: Chem.* **2014**, *192*, 607−627.
(8) Pokhel, S.; Simion, C. E.; Quemener, V.; Barsan, N.; Weimar, U. Investigations of Conduction Mechanism in Cr_2O_3 Gas Sensing Thick Films by AC Impedance Spectroscopy and Work Function Changes Measurements. *Sens. Actuators, B: Chem.* **2008**, *133*, 78−83.
(9) Hübner, M.; Simion, C. E.; Tomescu-Stănoiu, A.; Pokhel, S.; Barsan, N.; Weimar, U. Influence of Humidity on CO Sensing with P-type CuO Thick Film Gas Sensors. *Sens. Actuators, B: Chem.* **2011**, *153*, 347−353.
(10) Pirkanniemi, K.; Sillanpää, M. Heterogeneous Water Phase Catalysis as an Environmental Application: A Review. *Chemosphere* **2002**, *48*, 1047−1060.
(11) Bettahar, M. M.; Costentin, G.; Savary, L.; Lavalley, J. C. Review: On the Partial Oxidation of Propane and Propylene on Mixed Metal Oxide Catalysts. *Appl. Catal., A* **1996**, *145*, 1−48.
(12) Motooka, Y.; Ozaki, A. Regularities in Catalytic Properties of Metal Oxides in Propylene Oxidation. *J. Catal.* **1966**, *5*, 116−124.

(13) Kaye, S. S.; Long, J. R. Hydrogen Storage in the Dehydrated Prussian Blue Analogues $M_3[Co(CN)_6]_2$ (M = Mn, Fe, Co, Ni, Cu, Zn). *J. Am. Chem. Soc.* **2005**, *127*, 6506−6507.
(14) Shin, J. W.; Choi, S.-J.; Lee, I. K.; Youn, D. Y.; Park, C. O.; Lee, J.-H.; Tuller, H. L.; Kim, I. D. Thin-Wall Assembled SnO_2 Nanofibers Functionalized by Catalytic Pt Nanoparticles and Their Superior Exhaled Breath Sensing Properties for Diagnosis of Diabetes. *Adv. Funct. Mater.* **2013**, *23*, 2357−2367.
(15) Kolmakov, A.; Klenov, D. O.; Lilach, Y.; Stemmer, S.; Moskovits, M. Enhanced Gas Sensing by Individual SnO_2 Nanowires and Nanobelts Functionalized with Pd Catalyst Particles. *Nano Lett.* **2005**, *5*, 667−673.
(16) Kim, S.-J.; Hwang, I.-S.; Na, C.-W.; Kim, I.-D.; Kang, Y. C.; Lee, J.-H. Ultrasensitive and Selective C_2H_5OH Sensors Using Rh-Loaded In_2O_3 Hollow Spheres. *J. Mater. Chem.* **2011**, *21*, 18477−18488.
(17) Du, N.; Zhang, H.; Ma, X.; Yang, D. Homogeneous Coating of Au and SnO_2 Nanocrystals on Carbon Nanotubes via Layer-by-Layer Assembly: A New Termary Hybrid for a Room-Temperature CO Gas Sensor. *Chem. Commun.* **2008**, 6182−6184.
(18) Kugisima, M.; Shimanoe, K.; Yamazoe, N. C_2H_4O Sensing Properties for Thick Films Sensor Using La_2O_3-Modified SnO_2. *Sens. Actuators, B: Chem.* **2006**, *118*, 171−176.
(19) Na, C. W.; Woo, H.-S.; Kim, I.-D.; Lee, J.-H. Selective Detection of NO_2 and C_2H_5OH Using a Co_3O_4-Decorated ZnO Nanowire Network Sensor. *Chem. Commun.* **2011**, *47*, 5148−5150.
(20) Na, C. W.; Woo, H.-S.; Lee, J.-H. Design of Highly Sensitive Volatile Organic Compounds Sensors by Controlling NiO Loading to ZnO Nanowire Networks. *RSC Adv.* **2012**, *2*, 414−417.
(21) Woo, H.-S.; Na, C. W.; Kim, I.-D.; Lee, J.-H. Highly Sensitive and Selective Trimethylamine Sensor Using One-Dimensional ZnO-Cr_2O_3 Hetero-Nanostructures. *Nanotechnology* **2012**, *23*, 2445501.
(22) Cho, N. G.; Woo, H.-S.; Lee, J.-H.; Kim, I.-D. Thin-Walled NiO Tubes Functionalized with Catalytic Pt for Highly Selective C_2H_5OH Sensors Using Electrospun Fibers as a Sacrificial Template. *Chem. Commun.* **2011**, *47*, 11300−11302.
(23) Ando, M.; Kobayashi, T.; Iijima, S.; Haruta, M. Optical Recognition of CO and H_2 by Use of Gas-Sensitive Au-Co_3O_4 Composite Films. *J. Mater. Chem.* **1997**, *7*, 1779−1783.
(24) Kim, H.; Jin, C.; Park, S.; Kim, S.; Lee, C. H_2S Gas Sensing Properties of Bare and Pd-Functionalized CuO Nanorods. *Sens. Actuators, B: Chem.* **2012**, *161*, 594−599.
(25) Kim, H.-J.; Choi, K.-I.; Kim, K.-M.; Na, C. W.; Lee, J.-H. Highly Sensitive C_2H_5OH Sensors Using Fe-Doped NiO Hollow Spheres. *Sens. Actuators, B: Chem.* **2012**, *171*−*172*, 1029−1037.
(26) Yoon, J.-W.; Kim, H.-J.; Kim, I.-D.; Lee, J.-H. Electronic Sensitization of C_2H_5OH Response in P-Type NiO Nanofibers by Fe Doping. *Nanotechnology* **2013**, *24*, 444005.
(27) Lee, K. K.; Kang, Y. C.; Jung, K. Y.; Kim, J. H. Preparation of Nano-Sized $BaTiO_3$ Particle by Citric Acid-Assisted Spray Pyrolysis. *J. Alloys Compd.* **2005**, *395*, 280−285.
(28) Larson, A. C.; Von Dreele, R. B. *General Structure Analysis System (GSAS)*; Los Alamos National Laboratory Report LAUR 86-748; Los Alamos National Laboratory : Los Alamos, NM, 2004.
(29) Lin, F.; Nordlund, D.; Weng, T.-C.; Moore, R. G.; Gillaspie, D. T.; Dillon, A. C.; Richards, R. M.; Engtrakul, C. Hole Doping in Al-Containing Nickel Oxide Materials to Improve Electrochromic Performance. *ACS Appl. Mater. Interfaces* **2013**, *5*, 301−309.
(30) Kohl, D. Function and Applications of Gas Sensors. *J. Phys. D: Appl. Phys.* **2001**, *34*, R125.
(31) Yang, M.; Pu, H.; Zhou, Q.; Zhang, Q. Transparent P-type Conducting K-Doped NiO Films Deposited by Pulsed Plasma Deposition. *Thin Solid Films* **2012**, *520*, 5884−5888.
(32) Tseng, W. J.; Tsung, T.; Wu, H.-M.; Her, Y.-C.; Yang, T.-J. Facile Synthesis of Mono Dispersed In_2O_3 Hollow Spheres and Application in Photocatalysis and Gas Sensing. *J. Am. Ceram. Soc.* **2013**, *96*, 719−725.
(33) Donley, C.; Dunphy, D.; Paine, D.; Carter, C.; Nebesny, K.; Lee, P.; Alloway, D.; Armstrong, N. R. Chracterization of Indium-Tin Oxide Interfaces Using X-ray Photoelectron Spectroscopy and Redox Processes of a Chemisorbed Probe Molecule: Effect of Surface Pretreatment Conditions. *Langmuir* **2002**, *18*, 450−457.
(34) Park, S.; Ko, H.; Kim, S.; Lee, C. Role of the Interfaces in Multiple Networked One-Dimensional Core-Shell Nanostructured Gas Sensors. *ACS Appl. Mater. Interfaces* **2014**, *6*, 9595−9600.
(35) Tharsika, T.; Haseeb, A. S. M. A.; Akbar, S. A.; Sabri, M. F. M.; Hoong, W. Y. Enhanced Ethanol Gas Sensing Properties of SnO_2-Core/ZnO-Shell Nanostructures. *Sensors* **2014**, *14*, 14586−14600.
(36) Zhou, C.; Li, J.; Chen, S.; Wu, J.; Heier, K. R.; Cheng, H. First-Principles Study on Water and Oxygen Adsorption on Surface of Indium Oxide and Indium Tim Oxide Nanoparticles. *J. Phys. Chem. C* **2008**, *112*, 14015−14020.
(37) Golovanov, V.; Maki-Jaskan, M. A.; Tantala, T. T.; Korotcenkov, G.; Brinzari, V.; Cornet, A.; Morante, J. Experimental and Theoretical Studies of Indium Oxide Gas Sensors Fabricated by Spray Pyrolysis. *Sens. Actuators, B: Chem.* **2005**, *106*, 563−571.
(38) Song, X.; Gao, L.; Mathur, S. Synthesis, Characterization, and Gas Sensing Properties of Porous Nickel Oxide Nanotubes. *J. Phys. Chem. C* **2011**, *115*, 21730−21735.
(39) Lin, L.; Liu, T.; Miao, B.; Zeng, W. Synthesis of NiO Nanostructures from 1D to 3D and Researches of Their Gas-Sensing Properties. *Mater. Res. Bull.* **2013**, *48*, 449−454.
(40) Cho, N. G.; Hwang, I.-S.; Kim, H.-G.; Lee, J.-H.; Kim, I.-D. Gas Sensing Properties of P-Type Hollow NiO Hemispheres Prepared by Polymeric Colloidal Templating Method. *Sens. Actuators, B* **2011**, *155*, 366−371.
(41) Du, Y.; Wang, W.; Li, X.; Zhao, J.; Ma, J.; Liu, Y.; Lu, G. Preparation of NiO Nanoparticles in Microemulsion and Its Gas Sensing Performance. *Mater. Lett.* **2012**, *68*, 168−170.
(42) Zhao, C.; Fu, J.; Zhang, Z.; Xie, E. Enhanced Ethanol Sensing Performance of Porous Ultrathin NiO Nanosheets with Neck-Connected Networks. *RSC Adv.* **2013**, *3*, 4018−4023.
(43) Fu, J.; Zhao, C.; Zhang, J.; Peng, Y.; Xie, E. Enhanced Gas Sensing Performance of Eletrospun Pt-Functionalized NiO Nanotubes with Chemical and Electronic Sensitization. *ACS Appl. Mater. Interfaces* **2013**, *5*, 7410−7416.
(44) Zhu, G.; Xu, H.; Liu, Y.; Xi, C.; Yang, J.; Shen, X.; Zhu, J.; Yang, J. Platelet-Like Nickel Hydroxide: Synthesis and the Transferring to Nickel Oxide as a Gas Sensor. *J. Colloid Interface Sci.* **2013**, *412*, 100−106.
(45) Zhu, G.; Liu, Y.; Xi, C.; Bao, C.; Xu, H.; Shen, X.; Zhu, X. Polymer Guided Synthesis of $Ni(OH)_2$ with hierarchical Structure and Their Application as the Precursor for Sensing Materials. *CrystEngComm* **2013**, *15*, 9189−9195.